Cellular/Molecular

Dopamine D_2 Receptors Regulate Collateral Inhibition between Striatal Medium Spiny Neurons

Rupa R. Lalchandani,[1,2] Marie-Sophie van der Goes,[3] John G. Partridge,[2] and Stefano Vicini[2]

[1]Graduate Program in Physiology and Biophysics, [2]Department of Pharmacology & Physiology, [3]Department of Biology, Georgetown University, Washington, DC 20007

The principle neurons of the striatum are GABAergic medium spiny neurons (MSNs), whose collateral synapses onto neighboring neurons play critical roles in striatal function. MSNs can be divided by dopamine receptor expression into D_1-class and D_2-class MSNs, and alterations in D_2 MSNs are associated with various pathological states. Despite overwhelming evidence for D_2 receptors (D_2Rs) in maintaining proper striatal function, it remains unclear how MSN collaterals are specifically altered by D_2R activation. Here, we report that chronic D_2R stimulation regulates MSN collaterals *in vitro* by presynaptic and postsynaptic mechanisms. We used corticostriatal cultures from mice in which MSN subtypes were distinguished by fluorophore expression. Quinpirole, an agonist for $D_{2/3}$ receptors, was used to chronically activate D_2Rs. Quinpirole increased the rate and strength of collateral formation onto D_2R-containing MSNs as measured by dual whole-cell patch-clamp recordings. Additionally, these neurons were more sensitive to low concentrations of GABA and exhibited an increase in gephyrin puncta density, suggesting increased postsynaptic $GABA_A$ receptors. Last, quinpirole treatment increased presynaptic GABA release sites, as shown by increased frequency of sIPSCs and mIPSCs, correlating with increased VGAT (vesicular GABA transporter) puncta. Combined with the observation that there were no detectable differences in sensitivity to specific $GABA_A$ receptor modulators, we provide evidence that D_2R activation powerfully transforms MSN collaterals via coordinated presynaptic and postsynaptic alterations. As the D_2 class of MSNs is highly implicated in Parkinson's disease and other neurological disorders, our findings may contribute to understanding and treating the changes that occur in these pathological states.

Introduction

GABAergic medium spiny neurons (MSNs) mediate the integration of information within the striatum, ultimately controlling proper motor movement and behavior (Graybiel et al., 1994). Nearly 95% of all striatal neurons are GABAergic MSNs, which can be further divided by their differential dopamine (DA) receptor expression into D_1 or D_2 MSNs (Gerfen and Young, 1988; Bolam et al., 2000; Kreitzer and Malenka, 2008). As MSN axons branch extensively onto nearby neurons, MSNs have the capacity to tightly regulate striatal activity and output (Wilson, 1994; Plenz, 2003). Despite the overwhelming role for D_2 receptors (D_2Rs) in maintaining proper striatal function, it remains unclear how MSN collaterals are specifically altered by D_2R activation.

The D_2R is a G-protein-coupled receptor that is critical in maintaining proper function in the CNS (Girault and Greengard, 2004). Aberrant changes in D_2R expression and function in the striatum are closely related to schizophrenia, substance abuse, and obesity (Abi-Dargham et al., 2000; Volkow et al., 2001; Asensio et al., 2010; Johnson and Kenny, 2010). The D_2R is also the primary target of action for many antipsychotics (Seeman et al., 1975; Kapur et al., 2000) and for Parkinson's disease therapy (Lieberman and Goldstein, 1985). Interestingly, D_2 MSNs of the striatum have been shown to be the first population of neurons affected by DA depletion in Parkinsonism, resulting in alterations of D_2 MSN morphology and function (Albin et al., 1989; Day et al., 2006; Gittis and Kreitzer, 2012; Zold et al., 2012). In fact, recent evidence points to the specific reduction in D_2 MSN collaterals of the striatum in a mouse model of Parkinson's disease (Taverna et al., 2008).

To investigate the role of D_2R activation on GABAergic transmission, we developed a corticostriatal culture model using transgenic mice that express different fluorescent proteins to allow for simultaneous live identification of D_1 and D_2 MSNs [Gene Expression Nervous System Atlas project (GENSAT); Gong et al., 2003; Shuen et al., 2008]. An *in vitro* model allows for direct pharmacological control of DA receptor activation while maintaining neuronal integrity (Deyts et al., 2009). This provides the unique opportunity to specifically compare the effects of D_2R activation on the two major subtypes of striatal neurons. In the current study, we present direct evidence for the regulation of synaptic frequency and efficacy at MSN collateral synapses by chronic D_2R activation. Our data suggest that D_2R activation causes distinctive changes in MSN morphology with coordinated increases in the number of synaptic sites and density of postsyn-

Received Feb. 12, 2013; revised July 24, 2013; accepted July 28, 2013.

Author contributions: R.R.L., J.G.P., and S.V. designed research; R.R.L., M.-S.v.d.G., J.G.P., and S.V. performed research; R.R.L., M.-S.v.d.G., and S.V. analyzed data; R.R.L., J.G.P., and S.V. wrote the paper.

This work was supported by the National Institutes of Health (MH64797). We thank Filip Vanevski for sharing the ImageJ macros for puncta quantification.

The authors declare no competing financial interests.

Correspondence should be addressed to Rupa R. Lalchandani, Graduate Program in Physiology and Biophysics, Georgetown University School of Medicine, Basic Science Building Room 228, 3900 Reservoir Road NW, Washington, DC 20007. E-mail: rrl23@georgetown.edu.

DOI:10.1523/JNEUROSCI.0692-13.2013

 0270-6474/13/3314075-12$15.00/0

aptic $GABA_A$ receptor clusters. Together, our results demonstrate that GABAergic transmission between MSNs is significantly regulated by D_2R activation, and this occurs via coordinated presynaptic and postsynaptic modifications at specific MSN collaterals.

Materials and Methods

Corticostriatal cultures. We adapted the procedure originally described in Segal et al. (2003). BAC *drd1a*-tdTomato mice and BAC *drd2*-EGFP (enhanced green fluorescent protein) mice harbor bacterial artificial chromosome (BAC) transgenes with td-Tomato reporter downstream of D_1 receptor promoter and EGFP reporter downstream of the D_2 receptor promoter, respectively (GENSAT; Gong et al., 2003; Shuen et al., 2008). Crossing these two strains resulted in healthy mice pups, a subset of which coexpressed tdTomato in D_1 cells and EGFP in D_2 cells. Primary cultures were prepared from the progeny of this cross. Pups of either sex were decapitated at postnatal day 0 in accordance with the guidelines of the American Veterinary Medical Association Panel on Euthanasia and the Georgetown University Animal Care and Use Committee. Whole brains were removed and placed into ice-cold Krebs solution with 0.3% BSA, and subsequently examined for fluorophore expression using Dual Fluorescent Protein Flashlight (Nightsea). Striata from brains expressing both tdTomato and EGFP were dissected using GFP expression as a guide (Fig. 1*A*). Cortical tissue from littermates that did not express either fluorophore was separately dissected. Tissue was enzymatically (trypsin, 0.03%; Sigma-Aldrich) and mechanically dissociated to yield a single-cell suspension. Cells were diluted and combined to achieve a 1:3 ratio of cortical to striatal neurons at a final concentration of 5×10^5 cells/ml. Then, 250 μl of the cell suspension was plated onto poly-D-lysine (10 μg/ml; Sigma-Aldrich)-coated glass coverslips (1.13 cm^2). The coverslips had been previously incubated in Basal Eagle's medium (Invitrogen). Cells were cultured in Neurobasal medium supplemented 0.25% glutamine, 1% penicillin-streptomycin, 2% B27 (all from Invitrogen), 50 ng/ml BDNF (Alomone), and 30 ng/ml GDNF (Sigma-Aldrich; Gertler et al., 2008) and maintained at 37°C in 95% O_2/5% CO_2. At 2 d *in vitro* (DIV), one quarter of the medium was replaced with fresh Neurobasal medium with BDNF and GDNF as described above. Media was exchanged twice weekly, although BDNF and GDNF were not included after DIV 2 (Tian et al., 2010).

The *drd2*-EGFP line in our colony was backcrossed with a C57BL/6 line (Chan et al., 2012) to avoid the abnormalities reported in Kramer et al. (2011). The characteristics of MSNs in the presence and absence of treatments were also confirmed in cultures harvested from two separate mouse strains: *drd2*-cre;rosa26-tdTomato (Madisen et al., 2010) and *npy*-EGFP;*drd1a*-tdTomato (Shuen et al., 2008; Partridge et al., 2009). These mice were derived from FVB/B6/129/Swiss and C57BL/6- B6SJLF1 strains, respectively. As we did not detect any significant differences between strains, these data were excluded from the results section for consistency.

Treatments. Neurons were pharmacologically stimulated between DIV 18 and 21. To activate DA D_2 receptors, neurons were treated with the selective $D_{2/3}$ receptor agonist (±)-quinpirole dihydrochloride (10 μM; Sigma-Aldrich) diluted in Neurobasal media (Deyts et al., 2009). To study nonspecific actions of quinpirole, we pretreated a subset of coverslips for 10 min with $D_{2/3}$ receptor antagonist sulpiride (10 μM; Sigma-Aldrich). We then chronically treated the cells with 10 μM sulpiride plus 10 μM quinpirole for 72 h.

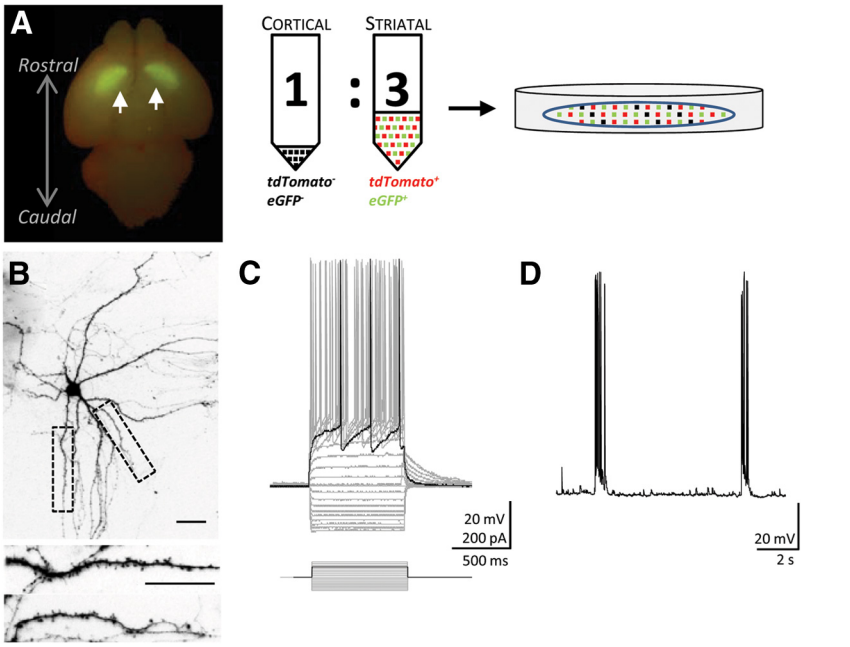

Figure 1. Corticostriatal cocultures from *drd1a*-tdTomato; *drd2*-EGFP mice. ***A***, Left, Dissected brain at postnatal day 0. Arrowheads indicate EGFP-positive striata in both hemispheres allowing for precise dissection. Right, Schematic of the culture preparation in which cells are dissociated and combined at a 1:3 ratio of cortical (nonfluorescing) to striatal (tdTomato and EGFP fluorescing) neurons. ***B***, A representative D_2 MSN at 15 DIV shows typical development of dendritic arbor (top) and formation of spines (insets, bottom). Calibration bars, 20 μm. ***C***, Voltage traces from an example D_2 MSN *in vitro* illustrates responses to step current injections. ***D***, Spontaneous membrane potential fluctuations at resting membrane potential reveal the regular occurrence of up and down states that were blocked by TTX (data not shown).

A smaller subset of coverslips was treated with a low dose of quinpirole (500 nM). Control neurons were given an equal volume of Neurobasal media without the addition of drug. All cells were returned to the incubator for 72 h before experimentation.

Electrophysiology. Whole-cell voltage-clamp and current-clamp recordings were performed on striatal neurons identified by either tdTomato or EGFP fluorescence. Cells were visualized with a Nikon TE-2000S inverted microscope with a 40× phase-contrast objective. All recordings were done at room temperature (RT) in extracellular solution (ES) continuously perfused at a rate of 2.5 ml/min. ES was composed of the following (in mM, except for phenol red), all from Fisher Scientific: 145 NaCl, 5 KCl, 1 $MgCl_2$, 1 $CaCl_2$, 5 HEPES, 5 glucose, 15 sucrose, phenol red (0.25 mg/L), adjusted to pH 7.4 with NaOH. Recording electrodes were pulled on a two-step vertical pipette puller (PP-83, Narishige) from borosilicate glass capillaries (Wiretrol II, Drummond) with resistances of 3–5 MΩ. To characterize basic electrophysiological properties, electrodes were filled with intracellular solution containing the following (in mM): 145 K-gluconate, 10 HEPES, 5 ATP · Mg, 0.2 GTP · Na, and 0.5 EGTA, adjusted to pH 7.2 with KOH. The equilibrium potential (E_{Cl-}) for Cl^- in this condition was −71.4 mV. To study inhibitory synaptic transmission, 100 mM K-gluconate plus 44 mM KCl was substituted for 145 mM K-gluconate. The E_{Cl-} for this solution was −29.6 mV, allowing GABAergic currents to be recorded as inward at −70 mV while preventing series resistance errors created by extremely large currents. The calculated liquid junction potentials for these conditions were 15.8 and 12.2 mV, respectively, and the values reported have been compensated accordingly. Whole-cell voltage-clamp recordings were performed with a Multiclamp 700B amplifier (Molecular Devices) and access resistance was monitored throughout the recordings. Currents were filtered at 1 kHz with an eight-pole low-pass Bessel filter and digitized at 5 kHz using an IBM-compatible microcomputer equipped with Digidata 1322A data acquisition board and pCLAMP10 software.

Stock solutions of bicuculline methobromide (BMR), tetrodotoxin (TTX), 2,3-dihydroxy-6-nitro-7-sulfamoyl-benzo[f]quinoxaline-2, 3-dione (NBQX; all from Abcam), and 4,5,6,7-tetrahydroisoxazolo[5,4-

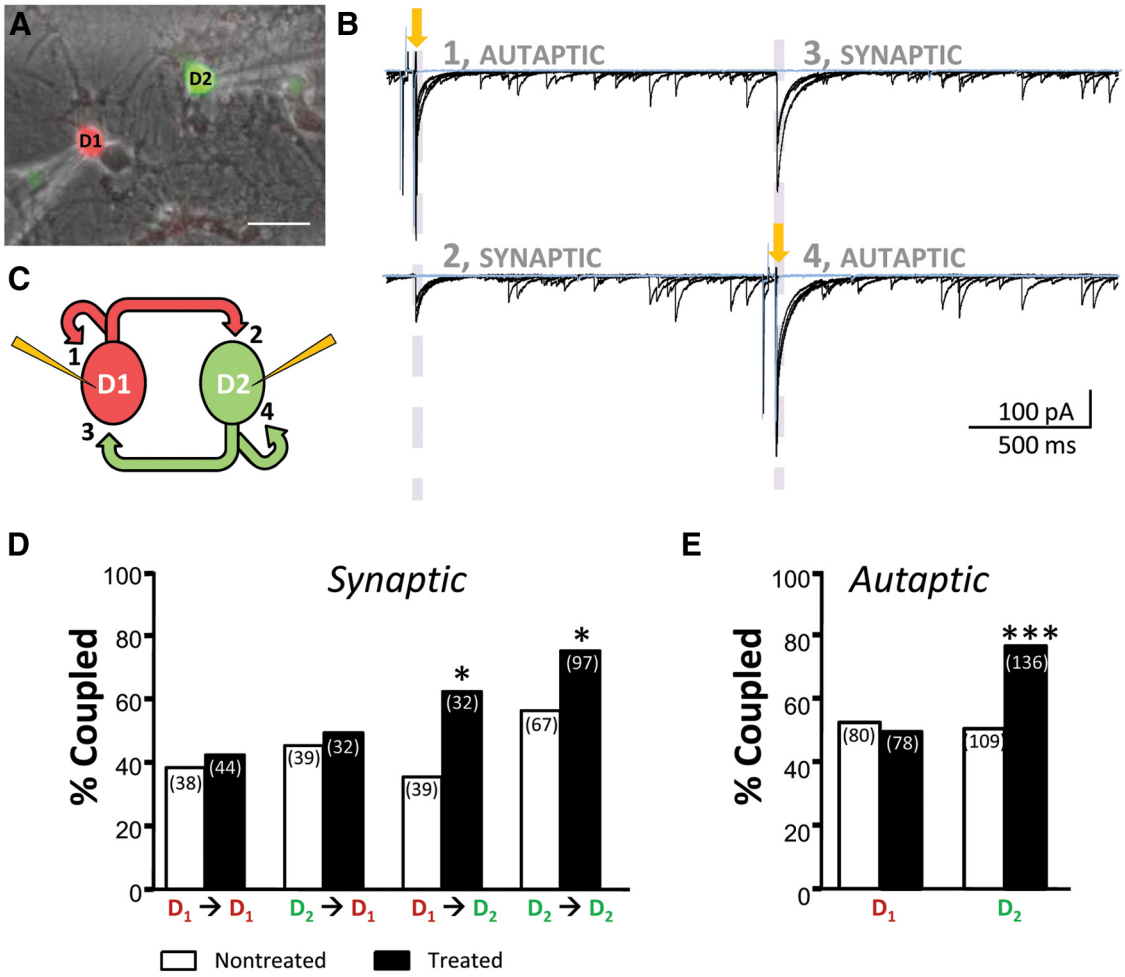

Figure 2. GABAergic synaptic connectivity between MSNs is sensitive to D_2R activation. ***A***, Superimposed GFP, RFP, and phase-contrast image of a D_1–D_2 MSN pair. Scale bar, 30 μm. ***B***, Example voltage-clamp traces from reciprocally coupled MSNs at 24 DIV. Yellow arrows mark the stimulation pulse. Dashed purple lines highlight both autaptic (1 and 4) and synaptic (2 and 3) responses. Local perfusion of 25 μM BMR (blue trace, superimposed) abolished all evoked and most spontaneous responses. ***C***, Schematic illustrating that a maximum of four synapses can be studied in a paired recording, as labeled, if the MSNs in the pair are both reciprocally connected and have autapses. ***D***, ***E***, Rates of connectivity between specific mature MSN pairs (21–24 DIV) at synapses (***D***) and autapses (***E***) exhibit an increased rate of synapse formation with 72 h 10 μM quinpirole treatment, exclusively when the postsynaptic neuron is a D_2 MSN. $^*p < 0.05$, $^{***}p < 0.001$; χ^2 test (total number of cells per pair tested in parentheses).

c]pyridin-3-ol (THIP; Sigma-Aldrich) were prepared in water and diluted in ES to a final concentration of 25 μM, 500 nM, 5, and 1 μM, respectively. Stock solutions of etomidate, flumazenil, and diazepam (all from Sigma-Aldrich) were prepared in dimethyl sulfoxide (DMSO) and diluted in ES (final DMSO concentration <0.01%). GABA (Sigma-Aldrich) was dissolved in water and diluted in ES to the desired concentrations. Solutions were rapidly exchanged using the Y-tube method (Murase et al., 1989).

Synaptic connections were studied in paired recordings while both neurons were held in voltage-clamp configuration at −70 mV. Cells were alternately stimulated at 3 s intervals with a voltage step to induce an action potential (+100 mV, 4 ms). Neurons were considered coupled if the presynaptic action potential induced an evoked IPSC (eIPSC) in the postsynaptic cell (Fig. 2*B*). Preceding stimulation, a test voltage pulse (−5 mV, 20 ms) was given to monitor series and input resistance and experiments with unstable holding currents were discarded. For variance–mean (V–M) analyses, changes in extracellular Ca^{2+} ($[Ca^{2+}]_o$) were induced with the Y-tube application of four $[Ca^{2+}]_o$ concentrations and resulting variances of eIPSC peaks were studied (Clements and Silver, 2000).

IPSC parameters were examined in Clampfit 10.2 (Molecular Devices). eIPSC averages were based on >20 events with failures removed. The decay phase of the averaged eIPSCs was fit to a double-exponential function and τ_w was calculated as the following:

$$\tau_w = \frac{A_1 \times \tau_1}{A_1 \times A_2} + \frac{A_2 \times \tau_2}{A_1 + A_2}$$

where τ_1 and τ_2 are the fast and slow decay time constants, respectively, and A_1 and A_2 are the contribution of the first and second exponentials to the amplitude (Nusser et al., 2001). Miniature (in TTX and NBQX) and spontaneous events were identified using semiautomated threshold-based software (Mini Analysis, Synaptosoft) and visually confirmed (Ade et al., 2008). More than 100 events were averaged per cell and decay kinetics were determined using a single-exponential equation.

Histochemistry. Anatomical reconstruction was achieved by including 1% biocytin in the intracellular solution of a subset of neurons (Partridge et al., 2009). To preserve the cell body, the pipette was carefully removed after 5–8 min to form an outside-out patch. Coverslips containing recorded, filled neurons were placed in 4% paraformaldehyde/4% sucrose/PBS solution for 15 min at RT, rinsed 3 times in 1× PBS and subsequently permeabilized and stained with fluorescein-avidin dye (Vector Labs) at 2.5 μl/ml for 120 min. Coverslips were briefly washed in PBS and mounted on glass slides using VectaShield antifade solution (H-1000, Vector Labs).

To better study D_2 MSN synapses, mature neurons were fixed and washed as described above. Next, coverslips were permeabilized and blocked, as in Tian et al. (2010), and incubated with antibodies to either rabbit α-GFP (1:200; Invitrogen) and mouse α-gephyrin (1:500; Synap-

Table 1. Membrane properties of mature D_1 and D_2 MSNs in primary cultures[a]

	Nontreated		Treated	
	D_1 MSN	D_2 MSN	D_1 MSN	D_2 MSN
Resting membrane potential (mV)	-73.9 ± 1.8 ($n = 22$)	-75.5 ± 1.5 ($n = 43$)	-75.1 ± 5.2 ($n = 9$)	-73.9 ± 1.4 ($n = 38$)
Input resistance (mΩ)	265 ± 18 ($n = 19$)	215 ± 23 ($n = 42$)	268 ± 27 ($n = 18$)	209 ± 20 ($n = 42$)
Capacitance (pF)	54 ± 5 ($n = 16$)	43 ± 4 ($n = 23$)	52 ± 4 ($n = 13$)	67 ± 5 ($n = 19$)***,+
Inward rectification index	1.7 ± 0.1 ($n = 8$)	1.7 ± 0.1 ($n = 22$)	2.0 ± 0.2 ($n = 8$)	2.1 ± 0.1 ($n = 13$)

[a]Whole-cell recordings from identified MSNs in nontreated and treated conditions showed that chronic D_2R activation increased the capacitance and inward rectification index in only D_2 MSNs. D_1 MSNs remained unchanged despite the treatment, serving as an internal control (data derived from at least 4 culture preparations). ***$p < 0.001$, comparing same cell type between treatment conditions using an unpaired *t* test; $^{+}p < 0.05$ comparing different cell types within a treatment condition using an unpaired *t* test.

tic Systems), or mouse α-GFP (1:500; Invitrogen) and rabbit α-VGAT (α vesicular GABA/glycine transporter; 1:1000; Abcam) for 2 h at RT. Appropriate secondary antibodies conjugated with Alexa-488 or Texas Red were diluted 1:1000. Coverslips were washed three times and mounted with VectaShield for visualization.

Microscopy and image analysis. Images of fixed and stained neurons at DIV 21–24 were acquired using a Nikon FS1 upright microscope equipped with a two-channel confocal imaging module (CLS-2HS, Thorlabs). Single confocal images were taken and basic morphological properties and Sholl analyses were conducted in ImageJ software [National Institutes of Health (NIH)].

Biocytin-injected cells were traced with the ImageJ NeuronJ plugin and dendritic arborization was analyzed with Sholl analysis plugin. Three to five neurons were analyzed per condition in three separate cultures and results were plotted as the number of intersections per 10 μm concentric circle from the soma.

Puncta measures were quantified with a custom macro for NIH ImageJ software (courtesy of F. Vanevski). Analyses were performed on puncta that were associated with either GFP+ or non-GFP neurons. One representative 70–100 μm dendritic segment was chosen per cell starting at the base of the primary dendrite. At least 10 neurons from different coverslips and cultures were analyzed for each condition. Puncta density and fluorescence intensity of immunoreactive puncta were calculated by thresholding images at two times background. Means from each representative dendrite per neuron were averaged to obtain population means.

Statistics. Kolmogorov–Smirnov tests were conducted on all datasets to check for normal distribution and appropriate statistics were chosen dependent upon these results. Statistical tests and graphical plots were performed in Prism 5 software (GraphPad) and are detailed in Results and figure legends. All data values in the text and figures are presented as mean ± SEM.

Results

Drd1a-tdTomato; *drd2*-EGFP corticostriatal cultures develop accurately *in vitro*

To perform a targeted study of D_1 and D_2 MSNs, we took advantage of *drd1a*-tdTomato*; drd2*-EGFP mice to further develop the model originally described by Segal et al. (2003) and extended by Tian et al. (2010). We cocultured striata that coexpressed EGFP and tdTomato with cortices from wild-type littermates; this avoided culturing cortical neurons that expressed fluorescently labeled D_1 and/or D_2 receptors. MSNs developed typical anatomical features in these culture conditions: by 2 weeks *in vitro*, neurons displayed extensive dendritic arborization and spiny protrusions (Fig. 1*B*). MSNs retained the expression of both fluorescent proteins *in vitro*, and mature neurons maintained a stable cell density of green, red, and nonfluorescent cells observed at densities of 43 ± 4, 49 ± 4, and 46 ± 6 cells/mm^2, respectively ($p > 0.05$; Friedman test). Interestingly, 11% of neurons (17 ± 3 cells/mm^2) coexpressed both fluorescent markers ($p < 0.0001$ compared with all other cell types; Friedman test). Neurons that expressed both fluorophores were not included in this study (data obtained in 79 fields from three culture preparations; DIV, >18).

To ensure that MSNs expressed characteristic electrophysiological properties, whole-cell patch-clamp recordings were performed from fluorescently identified D_1 and D_2 MSNs between DIV 21 and 24 using a potassium gluconate internal solution. Both MSN subtypes exhibited membrane properties reminiscent of those reported in brain slices (Dehorter et al., 2011), including action potential firing patterns, inward rectifying potassium currents, and the delay to first action potential suggestive of A-type potassium channel expression (Fig. 1*C*, Table 1). We also observed spontaneous membrane potential fluctuations that led to bursts of action potentials, likely due to up and down states as previously reported in organotypic slices (Plenz and Kitai, 1998) and dissociated cultures (Randall et al., 2011; Fig. 1*D*). Up and down states, paired with the occurrence of spines, suggest the successful innervation of MSNs by excitatory cortical neurons (Segal et al., 2003; Tian et al., 2010). The characteristics of MSNs observed in cultures from *drd1a*-tdTomato*; drd2*-EGFP remained consistent across three additional mouse strains and genotypes (*drd2*-EGFP, *drd2*-cre;*rosa26*-tdTomato, and *npy*-EGFP; *drd1a*-tdTomato; data not shown).

Paired recordings from MSN subtypes reveal reciprocal synaptic connectivity

Recurrent axon collaterals provide the striatal network with the capacity to integrate and store complex signals (Churchill and Sejnowski, 1992; Plenz, 2003). Thus, we investigated the occurrence of synaptic coupling between MSNs in our culture model. Concurrent whole-cell recordings were established from identified MSN pairs within the same visual field (Fig. 2*A*). As MSN synapses are GABAergic, pipettes were filled with an enhanced $[Cl^-]_i$ intracellular solution to achieve an E_{Cl-} at −30 mV (see Materials and Methods) to allow eIPSCs to be detected as inward. Cells were recorded in voltage-clamp at −70 mV and action potentials were artificially elicited in each cell to determine the presence of synaptic coupling. As seen in the example recording in Figure 2*B*, eIPSCs could be studied in this configuration. In addition to synaptic currents, we discovered the frequent occurrence of what appeared to be autaptic currents immediately following stimulation (Fig. 2*B*). Though autaptic currents were often detected in both recorded MSNs, this issue was not extensively pursued. Upon local perfusion with the $GABA_A$ receptor antagonist BMR (25 μM), both synaptic and autaptic currents were eliminated, demonstrating that activity from MSN collaterals in this preparation were indeed mediated by $GABA_A$ receptors (Fig. 2*B*, blue trace). eIPSCs were also blocked by perfusion with 0.5 μM TTX, and were unaffected by 5 μM NBQX (data not shown). Figure 2*C* shows a schematic of the potential synaptic arrangement between MSNs, revealing that a maximum of four synapses can be simultaneously studied in this configuration.

To determine whether eIPSCs were a result of direct monosynaptic or indirect polysynaptic connections, we examined eIPSC latency to peak and failure rate. MSNs consistently dis-

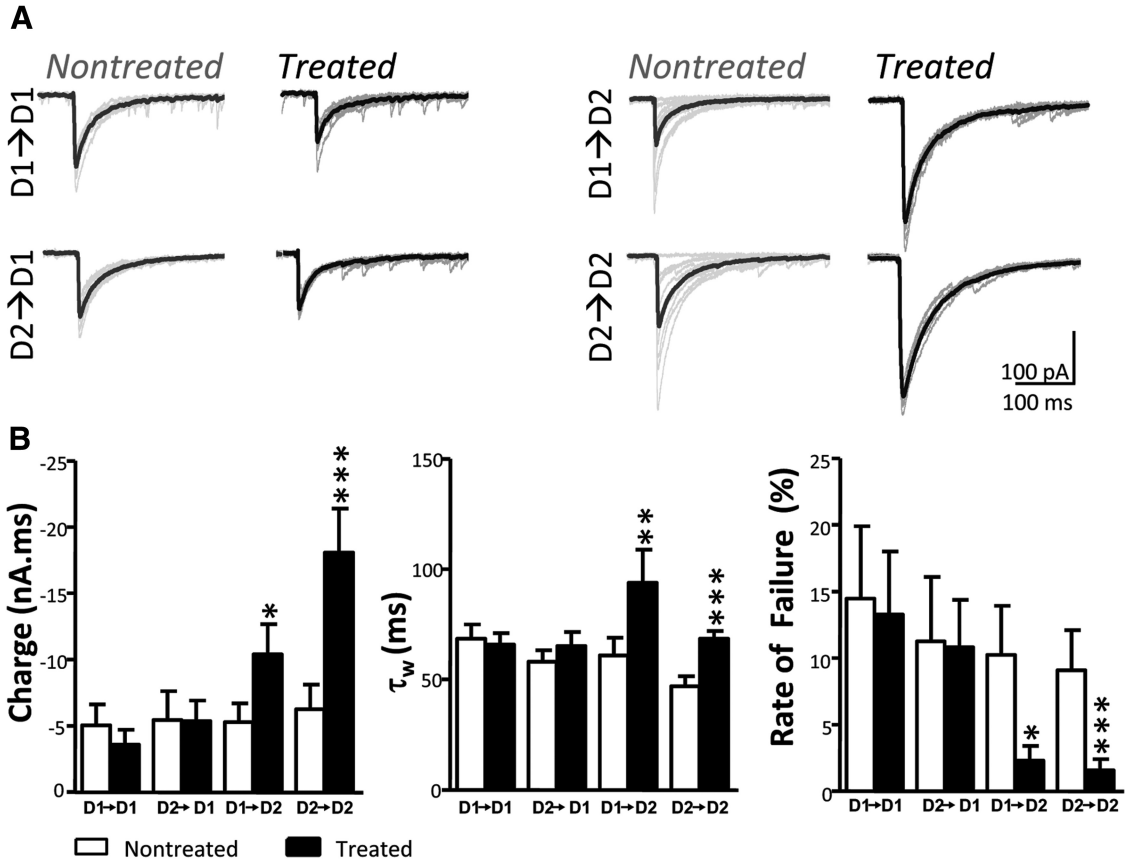

Figure 3. Chronic D_2R activation increases the strength of D_2 eIPSCs. ***A***, eIPSC traces with superimposed averages from representative pairs of MSN combinations in nontreated and treated conditions. ***B***, Summary plots compare charge transfer, fitted decay time constant (τ_w) and rate of failure, separated by experimental condition ($n = 13$ and 15 for D1–D1 nontreated and treated MSNs, respectively; $n = 19$ and 16 for D_2–D_1 nontreated and treated MSNs, respectively; $n = 16$ and 21 for D_1–D_2 nontreated and treated MSNs, respectively; $n = 22$ and 33 for D_2–D_2 nontreated and treated MSNs, respectively). $^*p < 0.05$, $^{**}p < 0.01$, $^{***}p < 0.001$; Mann–Whitney test.

played rapid and homogenous latency to peak (4.3 ± 0.2 ms), and low rates of failures (8.9 ± 2%), suggesting that eIPSCs were a result of direct monosynaptic connections ($n = 50$ cells from six culture preparations). Although we occasionally observed clear evidence of multipeaked, long-lasting eIPSCs suggestive of polysynaptic activity, we found this in <5% of the MSN pairs examined and these neurons were excluded from the study. A summary of the relative occurrence of the synaptic and autaptic currents detected between the two MSN subtypes is shown in Figure 2*D*,*E* (open bars).

Chronic D_2R activation increases coupling onto D_2 MSNs

It has been shown that MSN collaterals are negatively regulated by DA depletion (Taverna et al., 2008), but it remains unknown to which DA receptor these changes can be attributed. To investigate whether D_2R activation affects GABAergic coupling between MSN subtypes, we examined neurons in an environment where DA levels could be tightly regulated. As corticostriatal cultures are devoid of dopaminergic input, we treated mature cultures with the D_2R-class agonist quinpirole (10 μM) for 72 h. Pilot experiments determined this treatment regimen as optimal. Cultures treated with the D_1-class receptor agonist SKF (1 μM) and quinpirole (1 μM) at DIV 2 showed no difference in connectivity between D_2 MSNs at DIV 14 ($n = 10$ per condition, $p = 0.606$; χ^2 test). Although cultures treated with quinpirole (10 μM) at DIV 10 exhibited increased connectivity between D_2 MSNs by DIV 13 ($n = 8$ per condition, $p = 0.021$; χ^2 test), cultures >18 DIV were used for experimentation to avoid confounds that could be attributable to development *in vitro*. To address potential nonspecific effects of 10 μM quinpirole, we conducted additional paired recordings from coverslips cotreated with 10 μM quinpirole and 10 μM D_2R selective antagonist sulpiride. In this condition, D_2 MSNs were detected as coupled in 40% of 58 synaptic pairs, from two culture preparations ($p = 0.025$ when compared with nontreated D_2 MSN pairs; χ^2 test). Coverslips treated in parallel with 500 nM quinpirole exhibited 75% coupling in 28 pairs ($p = 0.156$ when compared with nontreated D_2 MSN pairs; χ^2 test).

We first examined whether chronic D_2R activation with 10 μM quinpirole altered the rate of functional synapse formation between MSN pairs. We observed that postsynaptic D_2 MSNs were more likely to receive coupling in the treated condition, regardless of presynaptic partner (Fig. 2*D*). Interestingly, the rate of autapse formation also increased with quinpirole treatment, again in exclusively D_2 MSNs (Fig. 2*E*). In support of this observed increase in connectivity, the likelihood in which two D_2 neurons were reciprocally coupled was also significantly increased: while reciprocal connections were found in 26 of 67 (39%) cells analyzed in nontreated conditions, reciprocal connections increased to 60 of 97 (62%) analyzed cells after chronic D_2R activation ($p = 0.004$; χ^2 test).

We compared the size and kinetics of eIPSCs between the two conditions to study changes in synapse strength following quinpirole treatment. Charge transfer and time to decay (τ_w) increased in treated D_2 MSNs, regardless of presynaptic partner

(Fig. 3*A*,*B*). Similar results were seen for peak amplitude in D_2 MSNs (-89 ± 22, $n = 35$ cells to -191 ± 25, $n = 54$ cells, $p = 0.0002$; Mann–Whitney test) but not D_1 MSNs (-74 ± 20, $n = 32$ cells to -96 ± 24, $n = 31$ cells, $p = 0.213$; Mann–Whitney test). These results correlated with a decrease in failure rate (Fig. 3*B*), as well as a decrease in coefficient of variation for postsynaptic D_2 MSNs (0.50 ± 0.05, $n = 45$ cells to 0.34 ± 0.02, $n = 55$ cells, $p = 0.007$; Mann–Whitney test) but not D_1 MSNs ($0.42 \pm 0.04\%$, $n = 30$ cells to 0.39 ± 0.02, $n = 27$ cells, $p = 0.867$; Mann–Whitney test). Together, paired recordings from identified MSNs suggest that activation of the D_2R increases the rate of collateral formation onto D_2 MSNs and these collaterals form larger, longer, and more reliable eIPSCs when compared with nontreated controls.

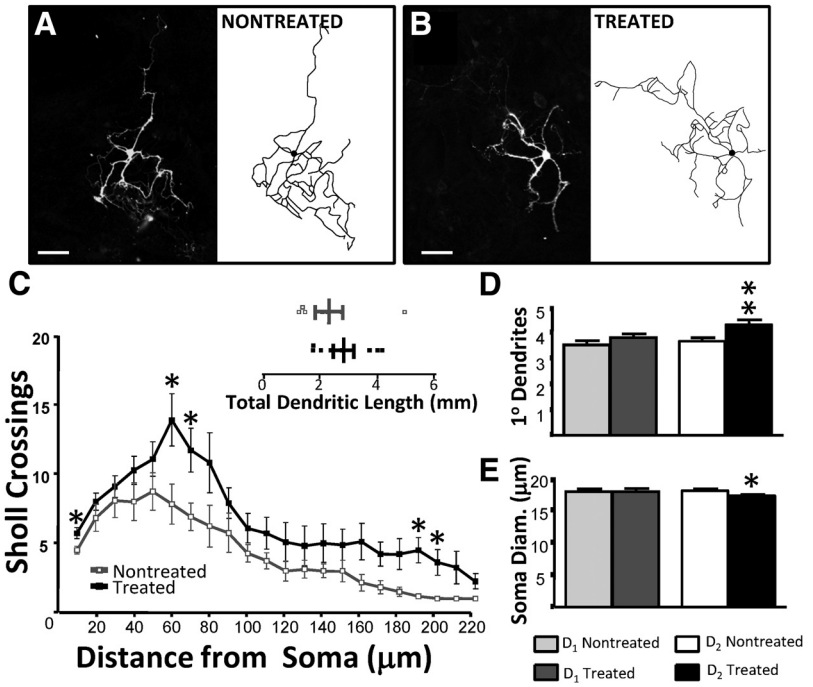

Figure 4. D_2R activation increases dendritic complexity. ***A***, ***B***, Biocytin-injected (left) and traced (right) nontreated (***A***) and treated (***B***) D_2 MSNs. Scale bar, 50 μm. ***C***, Analysis of Sholl crossings and dendrite lengths reveals an increase in primary dendrites and enhanced number of crossings with no change in dendritic length (inset). There was a significant main effect of the treatment ($p < 0.0001$) and of distance from the soma ($p < 0.0001$). Sholl crossings were analyzed with two-way ANOVA and Bonferroni's post-test, and individual points and dendritic length were analyzed with unpaired *t* tests ($n = 11$–12/condition from 3 cultures). ***D***, Dendrite counts from phase-contrast images confirms a significant increase in number of primary dendrites in treated D_2 MSNs (Mann–Whitney test). ***E***, Soma diameter of D_2, but not D_1, MSNs decreases slightly in the treated condition ($n > 28$ cells/group, $^*p < 0.05$; unpaired *t* test).

D_2R activation influences D_2 MSN morphology and synapse formation

It has been previously reported that the presence of DA alters D_2 MSN morphology (Gertler et al., 2008, Day et al., 2008). We therefore examined whether quinpirole treatment altered D_2 MSN morphology in a subset of MSNs ($n = 11$–12/condition from three cultures). Biocytin injections allowed for morphological reconstruction and subsequent analysis of the dendritic arbor (Fig. 4*A*,*B*). A plot of dendritic complexity (Fig. 4*C*) illustrates slight but significant increases in dendritic arborization with the treatment. Analysis of phase-contrast images confirms an increase in primary dendrite number (Fig. 4*D*) and reports a reduction in soma diameter (Fig. 4*E*) in treated D_2 MSNs while D_1 MSNs remain unchanged ($n > 50$/condition).

As increased dendritic arborization may improve the likelihood of synapse formation, we studied possible alterations in presynaptic terminals using α-VGAT antibody, which is a marker for vesicular GABA transporter. D_2 MSNs showed an increase in VGAT puncta density after D_2R activation specifically in GFP-labeled dendrites (Fig. 5*A*,*B*). A correlated increase in the frequency of spontaneous (Fig. 5*C*,*E*) and miniature (Fig. 5*D*,*E*) IPSC events was also observed. D_1 MSNs displayed no change in mIPSC frequency (2.3 ± 1.5, $n = 8$ cells to 2.15 ± 0.5, $n = 8$ cells, $p = 0.869$; unpaired *t* test). As no change in peak amplitude of mIPSCs was noted in D_2 MSNs between treatments, the smaller average sIPSC peak and increased mIPSC frequency are possibly the result of a preferential increase in small events in the treated condition (Fig. 5*F*). τ_w was not significantly affected by D_2R activation (Fig. 5*G*). It is important to keep in mind that mIPSCs and sIPSCs need not originate exclusively from MSNs; striatal or cortical interneurons could contribute as well. Quantal content, determined by dividing the average amplitude of eIPSCs by the average mIPSC per cell, was also significantly affected in D_2 MSNs (6.9 ± 1.8, $n = 14$ cells to 16.4 ± 2.7, $n = 32$ cells, $p = 0.030$; unpaired *t* test) but not in D_1 MSNs (8.2 ± 1.6, $n = 10$ cells to 7.4 ± 5.1, $n = 5$ cells, $p = 0.853$; unpaired *t* test). The increase in quantal content and the decrease in failure rate of treated D_2 MSN eIPSCs further supports a potential increase in either the number of release sites or the release probability following quinpirole treatment.

To evaluate these two possibilities, we used a V–M analysis of eIPSC amplitudes as described by Clements and Silver (2000). The relationship between amplitude variation and amplitude mean with changes in external calcium concentrations ($[Ca^{2+}]_o$) can be plotted to determine quantal size (Q), number of release sites (N), and the average probability of vesicular transmitter release (P_r). As expected, changing $[Ca^{2+}]_o$ from 0 to 0.5 mM and then to 1 mM led to increases in eIPSC amplitude variance and amplitude mean in D_2 neurons from both treated and nontreated conditions. When $[Ca^{2+}]_o$ was increased to 2 mM $[Ca^{2+}]_o$, nontreated D_2 MSNs again displayed an increase in eIPSC amplitude variance and amplitude mean (Fig. 6*A*). D_2 MSNs in the treated condition, on the other hand, exhibited an increase in eIPSC amplitude mean but a reduction of amplitude variance (Fig. 6*B*). As illustrated in Figure 6*C*, the V–M plot of D_2 MSNs in the nontreated condition was relatively linear, indicating increased variance at higher $[Ca^{2+}]_o$ concentrations. On the other hand, the V–M plot of treated D_2 MSNs formed a distinct parabola (Fig. 6*D*). These data support the hypothesis that D_2R activation via quinpirole increases the number of GABA release sites (N) or vesicular GABA release probability (P_r). However, the lack of parabolic mean–variance relationship in the nontreated condition prevents us from truly distinguishing between these two possibilities.

As the effects of the treatment on eIPSCs were observed only when the postsynaptic target was a D_2 MSN, we hypothesize that D_2R activation preferentially affects postsynaptic D_2 MSNs, independent of the presynaptic partner. The increased frequency of sIPSC and mIPSC events in quinpirole-treated D_2 MSNs, along with the reduction in failures of eIPSCs, suggests an increase in the number of MSN collaterals and a potential increase in clusters of postsynaptic $GABA_A$ receptors.

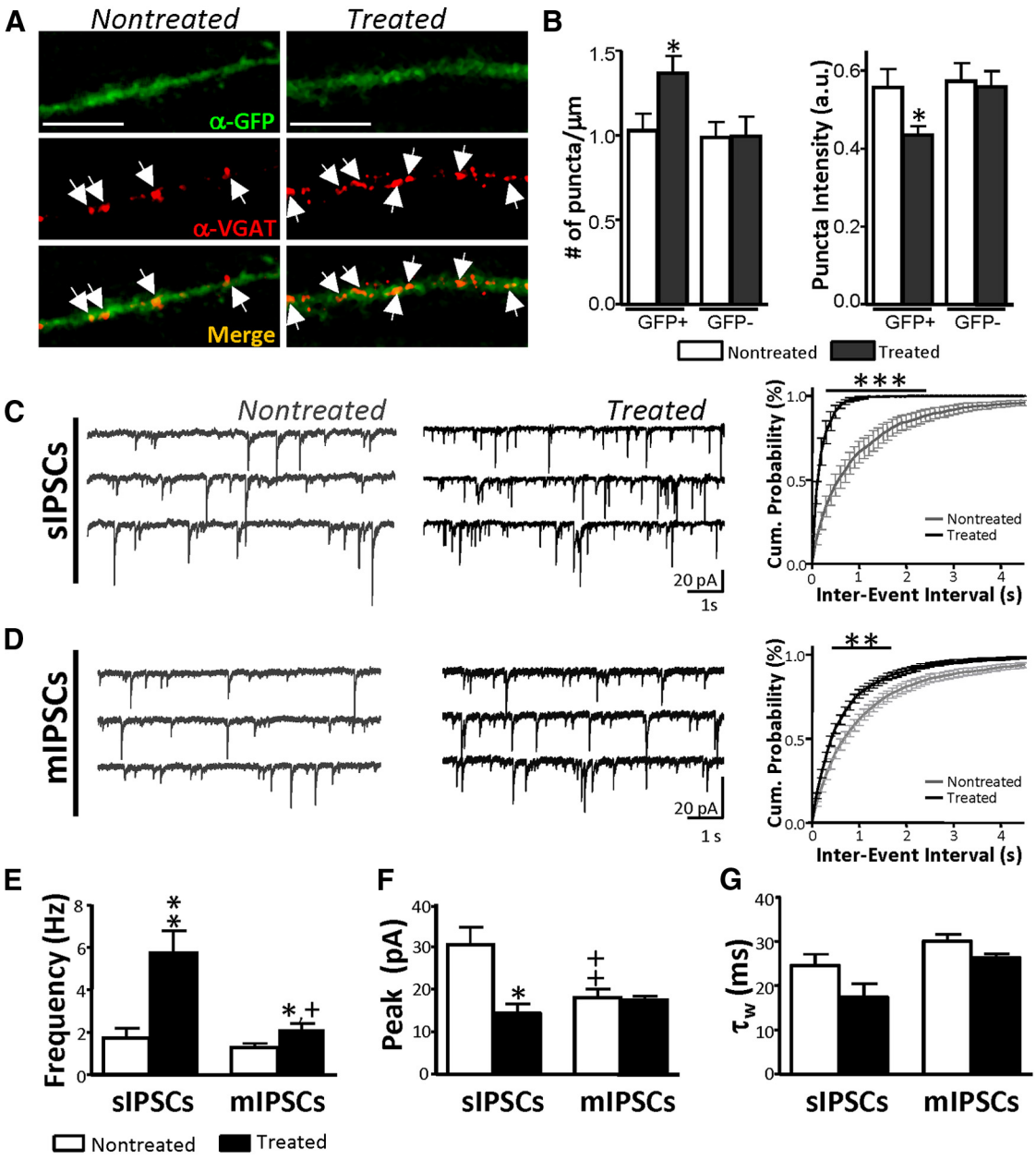

Figure 5. D_2R activation increases number of presynaptic terminals. ***A***, Confocal images of nontreated (left) and treated (right) D_2 MSN segments, stained against GFP (green) and VGAT (red). Scale bar, 5 μm. ***B***, VGAT puncta density (left) and puncta intensity (right) in identified GFP + and GFP − dendrites as quantified in ImageJ (*$p < 0.05$; Mann–Whitney *U* test). ***C***, ***D***, Representative sIPSC (***C***) and mIPSC (***D***) traces from D_2 MSNs recorded from nontreated (left) and treated (middle) D_2 MSNs. Plots of cumulative interevent intervals in D_2 MSNs (right) show a reduction in time between events in treated D_2 neurons. ***E–G***, Summary plots compare frequency (***E***), peak amplitude (***F***), and τ_w (***G***) of sIPSCs and mIPSCs in D_2 MSNs in both experimental conditions ($n = 38$ and 55 nontreated and treated cells/group). D_1 MSNs similarly exhibited no change in kinetics or amplitude (data not shown). *$p < 0.05$ when comparing mIPSCs or sIPSCs between treatment condition (Mann–Whitney *U* test). $^{++}p < 0.01$ when comparing mIPSCs and sIPSCs within treatment group (Wilcoxon signed-rank test).

Chronic D_2R activation increases GABA sensitivity of D_2 MSNs

We therefore examined postsynaptic $GABA_A$ receptor clusters with an α-gephyrin antibody. Gephyrin is a synaptic anchoring protein that colocalizes with postsynaptic $GABA_A$ and glycine receptors (Sassoè-Pognetto et al., 2000). Immunohistochemical analysis of gephyrin clusters in D_2 MSN dendrites revealed a significant increase of gephyrin puncta density after quinpirole treatment in exclusively D_2 MSN dendrites (Fig. 7*A*,*B*), supporting a postsynaptic increase of $GABA_A$ receptors with chronic D_2R activation.

To directly assess changes in $GABA_A$ receptor expression, we investigated the action of several GABA concentrations (0.3, 1, 3, and 10 μM) on whole-cell currents in D_1 and D_2 MSNs. In the nontreated condition, D_1 and D_2 MSNs exhibited similar sensitivity to all concentrations of GABA. With chronic quinpirole treatment, however, D_2 MSNs displayed a higher sensitivity at 0.3 and 1 μM GABA (Fig. 7*C–E*). Similarly, at 3 μM GABA, currents were 94 ± 33 pA, $n = 12$, and 250 ± 65 pA, $n = 11$, in nontreated and treated D_2 MSNs, respectively ($p = 0.032$; Mann–Whitney test). At 10 μM, currents were 201 ± 39 pA, $n = 23$, and 313 ± 46 pA, $n = 29$, in nontreated and treated D_2 MSNs, respectively ($p = 0.074$; Mann–Whitney test). The larger currents in response to GABA in treated D_2 MSNs point strongly to a postsynaptic mechanism for DA, but whether this is due to an increase in $GABA_A$ receptor number, as suggested by increased gephyrin clusters, or a change in $GABA_A$ receptor subtype required further elucidation.

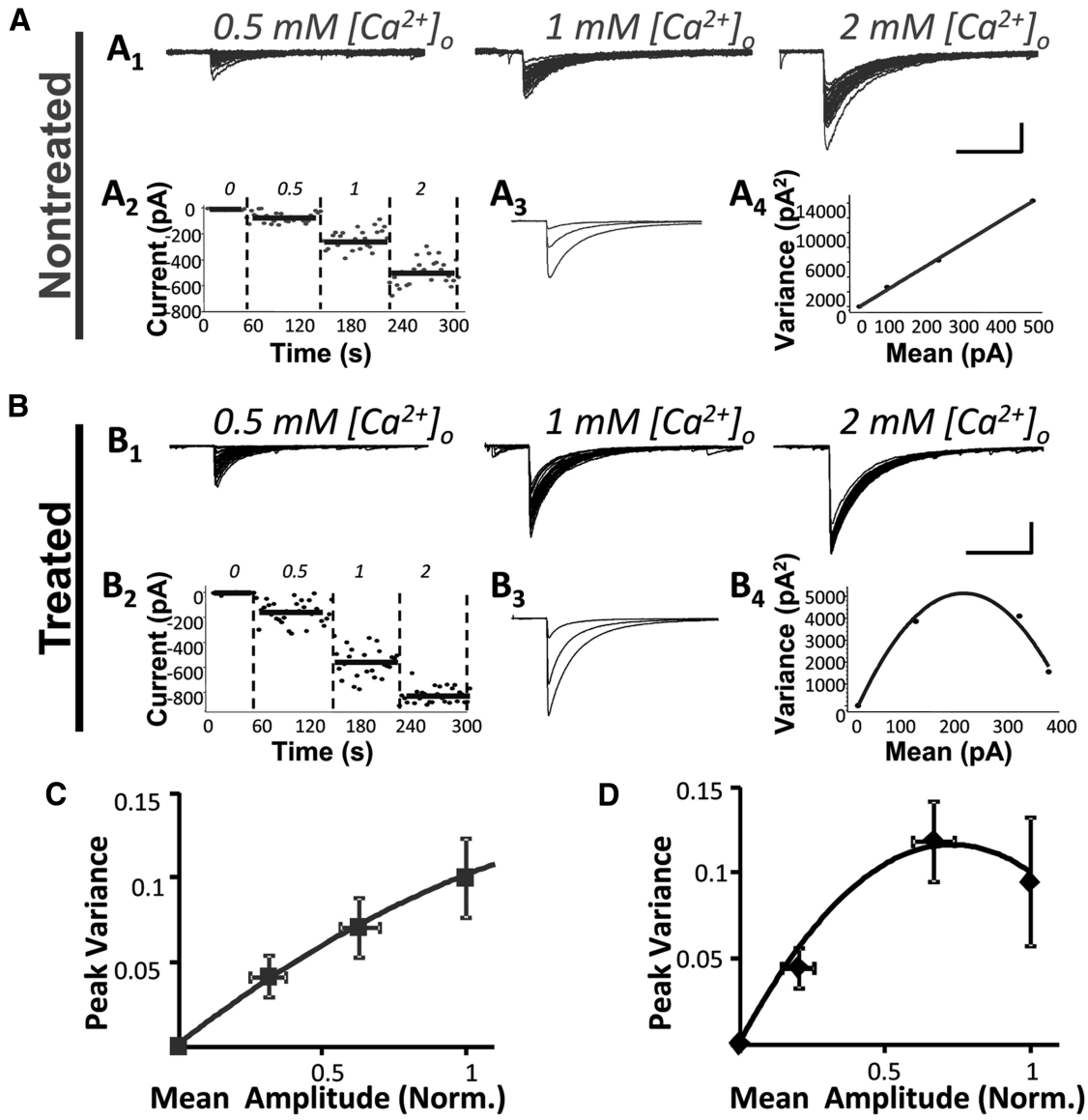

Figure 6. V–M analysis of eIPSC amplitudes. ***A***, ***B***, V–M analyses of eIPSCs from a single representative nontreated (***A***) and treated (***B***) D_2 MSNs. A_1, B_1, Superimposed eIPSCs illustrate amplitude fluctuations with changes in external calcium ($[Ca^{2+}]_o$) concentration. A_2, B_2, The time course of individual responses is plotted with four $[Ca^{2+}]_o$ concentrations as indicated. A_3, B_3, Mean peak values are overlayed per concentration. A_4, B_4, V–M plots generated per cell highlight differences in release probabilities between conditions. ***C***, ***D***, Summary data show contrasting V–M trends between nontreated (***C***) and treated (***D***) conditions, suggesting higher release probability in D_2 MSNs treated with quinpirole. V–M is normalized to the mean value of 2 mM Ca^{2+} in each cell (n = 13 and 10 cells/group from 4 culture preparations). Scale bars: x-axis, 150 ms; y-axis, 100 pA.

Different $GABA_A$ receptor subunits influence receptor conductance, open probability, and ligand affinity (Macdonald and Olsen, 1994). The δ subunit-containing extrasynaptic $GABA_A$ receptor has been shown to be more sensitive to GABA (Farrant and Nusser, 2005). As D_2 MSNs displayed increased GABA sensitivity with the quinpirole treatment, we hypothesized that this may be a result of increased expression of the δ subunit-containing $GABA_A$ receptor. THIP, a preferring agonist for δ subunit-containing $GABA_A$ receptor, was locally perfused while MSNs were in whole-cell configuration. Response to 1 μM THIP did not significantly change with the quinpirole treatment in either MSN subtype (Fig. 7*C*,*D*). Interestingly, D_2 MSNs exhibited larger currents in response to THIP compared with D_1 MSNs, suggesting a greater expression of extrasynaptic $GABA_A$ receptors in D_2 MSNs basally *in vitro* (Fig. 7*E*). Synaptic $GABA_A$ receptors in the striatum contain the β3 subunit (Janssen et al., 2011). Etomidate has been shown to consistently modulate the β2/3 subunit-containing $GABA_A$ receptor and was therefore used to assess any potential changes in synaptic $GABA_A$ receptors. As with THIP, there were no detectable differences in peak current responses to etomidate within MSN subtype when compared between conditions (Fig. 7*C*,*D*).

These experiments suggest that the increased sensitivity to GABA observed in quinpirole-treated D_2 MSNs is not related to changes in β2/3 or δ subunit expression. Thus, together, the increase in mIPSC frequency and GABA sensitivity point to an increase in number of postsynaptic $GABA_A$ receptors with treatment. As we did not observe a correlated increase in mIPSC amplitude, the data point to an increase in the number of inhibitory synaptic sites with chronic D_2R stimulation. Although we cannot exclude a preferential increase in other $GABA_A$ receptor subtypes, or postsynaptic modifications of existing receptors, the most plausible explanation is an increase in the density of $GABA_A$ receptor clusters with quinpirole treatment.

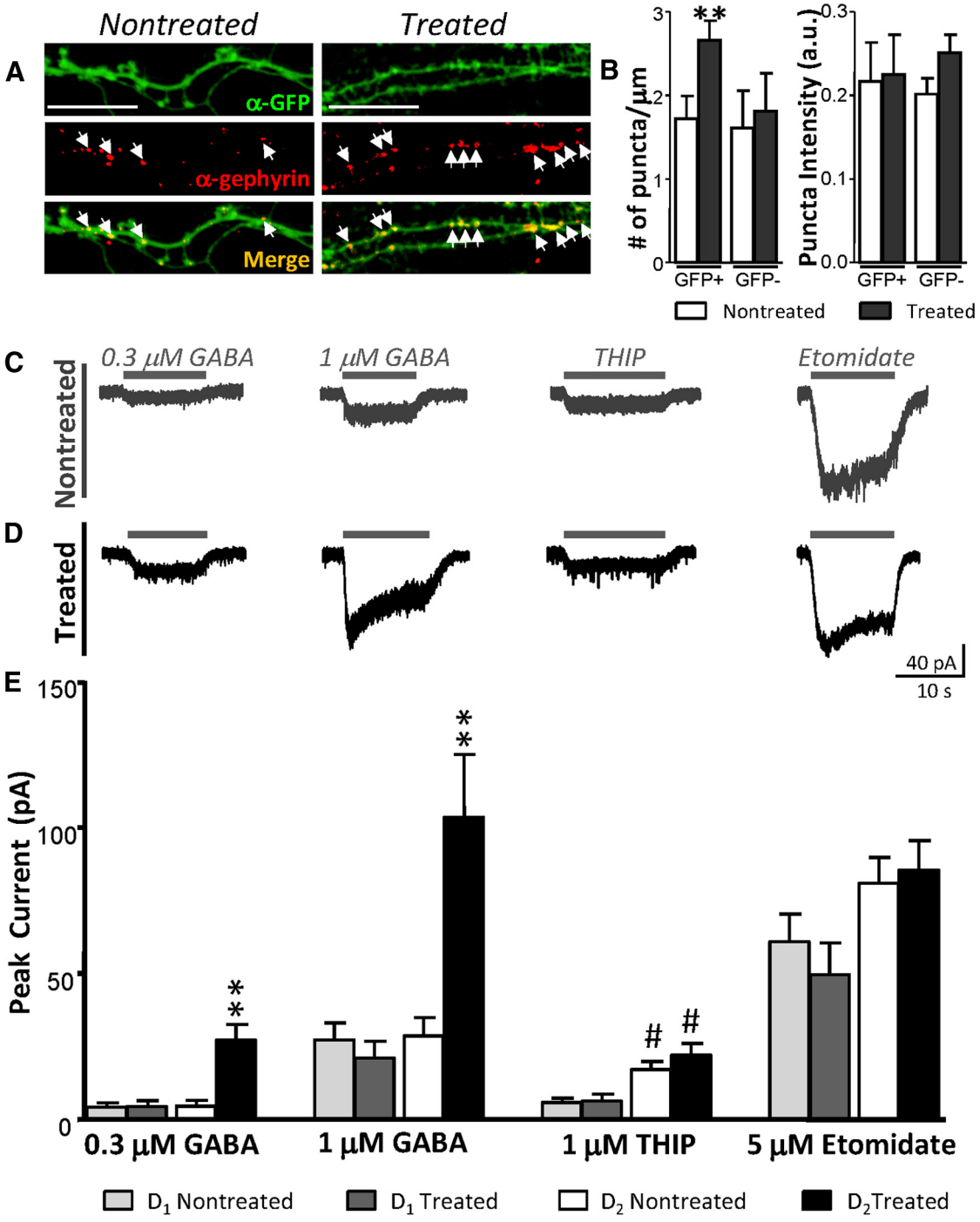

Figure 7. Enhanced $GABA_A$ sensitivity in D_2 MSNs following D_2R activation. ***A***, Confocal images of D_2 MSN segments with GFP (green) and gephyrin (red) staining in nontreated (left) and quinpirole-treated (right) conditions. Scale bar, 5 μm. ***B***, Summary plots of gephyrin puncta density (left) and puncta intensity (right) of identified GFP+ and GFP− dendrites (**$p < 0.01$; Mann–Whitney *U* test). ***C***, ***D***, Representative currents in response to direct Y-tube application of GABA, THIP (1 μM), and etomidate (5 μM) in nontreated (***C***) and treated (***D***) D_2 MSNs. ***E***, Summary of direct drug effects in D_1 and D_2 MSNs in each experimental condition ($n = 16–24$ cells/group; Kruskal–Wallis test with Dunn's post test: *$p < 0.05$, **$p < 0.01$, ***$p < 0.001$ comparing the same cell type between conditions; $^{\#}p < 0.05$, $^{\#\#}p < 0.01$ comparing different cell types within conditions).

Pharmacology of inhibitory synaptic connections between MSNs

To further investigate changes in $GABA_A$ receptor subtypes, we used benzodiazepine pharmacology. Benzodiazepine sensitivity relies on the presence of specific α and $\gamma 2$ subunits to increase frequency of opening of the targeted $GABA_A$ receptor subtypes (Macdonald and Olsen, 1994). If the targeted subunit is present, an enhancement of IPSC decay time (τ_w) is expected.

Flumazenil, a potentiator of $\alpha 4$, $\beta 3$, and $\gamma 2$ subunit-containing $GABA_A$ receptors (Ramerstorfer et al., 2010), failed to prolong IPSC decay in either condition, excluding a role for the $\alpha 4$ subunit (data not shown). Diazepam acts as a positive allosteric modulator at the benzodiazepine site of $\alpha 1$–3-containing or $\alpha 5$-containing $GABA_A$ receptors. Local perfusion of 5 μM diazepam revealed a prolongation of eIPSCs in both nontreated and treated D_2 MSNs, indicating that D_2 MSNs in both conditions

express these subunits (in nontreated D_2 MSNs, τ_w increased from 38 ± 3 to 48 ± 3 ms, $n = 5$, $p = 0.025$, paired t test; in treated D_2 MSNs, τ_w increased from 56 ± 5 to 79 ± 3 ms, $n = 8$, $p = 0.035$, paired t test). Interestingly, the increase in τ_w of eIPSCs from baseline was larger in quinpirole-treated (41%) versus nontreated (23%) D_2 MSNs ($p < 0.0001$; unpaired t test). Amplitude of eIPSCs was not affected by the presence of the benzodiazepine (data not shown).

To investigate whether quinpirole treatment induced a greater expression of benzodiazepine-sensitive $GABA_A$ receptors over other $GABA_A$ receptor subtypes, we studied the effect of diazepam on mIPSCs. As an mIPSC reflects the response to a single quantum of neurotransmitter, if benzodiazepine-induced prolongation of mIPSC τ_w was enhanced following quinpirole, this would suggest increased relative expression of diazepam-sensitive $GABA_A$ receptors. We observed that diazepam significantly prolonged mIPSC decay: in nontreated D_2 MSNs, τ_w increased from 25 ± 2 to 33 ± 1 ms, $n = 12$ ($p < 0.0001$; paired t test); in treated D_2 MSNs, τ_w increased from 27 ± 3 to 39 ± 3 ms, $n = 8$ ($p < 0.0001$; paired t test). However, unlike eIPSCs, the diazepam-induced change in mIPSC τ_w did not differ between conditions (32% nontreated and 44% quinpirole-treated, $p = 0.08$; unpaired t test). The possibility that mIPSCs and eIPSCs may be derived from different presynaptic terminals should be considered. However, the slower decay of eIPSCs compared with mIPSCs suggests they reflect asynchronous summation of multiple synaptic currents produced at distinct sites (Mody et al., 1994). Thus, the enhanced effect of diazepam on eIPSCs compared with mIPSCs in treated D_2 MSNs may be due to increased number of synaptic connections on D_2 MSNs with chronic quinpirole treatment.

Discussion

Collateral inhibition between MSNs allows for proper integration of information within the striatum (Czubayko and Plenz, 2002; Tunstall et al., 2002; Koos et al., 2004; Gustafson et al., 2006; Tecuapetla et al., 2007). Using paired patch-clamp recordings from identified MSNs *in vitro*, our results provide evidence for three novel conclusions. First, D_2R activation with chronic quinpirole treatment increases the frequency and strength of synapse formation in postsynaptic D_2 MSNs. These functional synapses are stronger and more reliable, and they exhibit substantially prolonged decay time. Second, quinpirole-treated D_2 MSNs display increased dendritic complexity, a morphological change that may enhance the likelihood of synapse formation. Third, an increased GABA sensitivity without obvious changes in $GABA_A$ receptor subtype suggests an increase in postsynaptic $GABA_A$ receptor number with this treatment. Together, our data indicate that chronic D_2R activation results in a greater synaptic efficacy via a coordinated increase of synaptic $GABA_A$ receptor clusters and GABA release sites.

MSN collaterals *in vitro*

An *in vitro* model that allows for simultaneous identification of both MSN subtypes is useful for the targeted investigation of the role of D_2Rs in striatal networks. We report that corticostriatal cultures from *drd1a*-tdTomato; *drd2*-EGFP mice retain their fluorescent properties through time *in vitro*. Neurons in these cocultures have profiles comparable to MSN development observed *in vivo*, including action potential firing patterns, up-and-down states, developed dendritic morphology, and spine formation. MSNs in our primary culture concurrently display properties that are not typically seen *ex vivo*, such as autaptic currents and colocalization of D_2 and D_1 MSNs markers. The absence of natural targets for MSNs in culture may explain the high rate of autapse formation, as is exemplified with *in vitro* microislands (Bekkers, 2005). The considerable extent of neurons that coexpress both D_1 and D_2 markers in primary culture may be a consequence of harvesting MSNs at an early developmental stage (Goffin et al., 2010).

Studies of striatal MSNs in primary culture or organotypic slice models (Plenz and Aertsen, 1996; Segal et al., 2003; Gertler et al., 2008; Tian et al., 2010; Kaufman et al., 2012) offer advantages and disadvantages compared with acute slice preparations. Primary cultures enable manipulation of the extracellular environment and consequently allow close comparisons between experimental conditions. In addition, *in vitro* models are useful to distinguish cell-autonomous contributing factors from environmental contributing factors (Gertler et al., 2008). These benefits come with inherent limitations: dissociated culture models disrupt the natural development of cytoarchitecture, potentially altering cellular and network phenotypes. However, while *in vitro* culture models report enhanced rates of functional connectivity, *ex vivo* slice preparations unavoidably reduce the estimated extent of coupling due to slice thickness and depth of neurons (Chuhma et al., 2011). Therefore, *in vitro* preparations are useful for dissecting out changes in MSN collaterals.

Lack of DA *in vivo* has been found not to affect the development of MSNs or proper neural circuits in a DA-deficient mouse model (Zhou and Palmiter, 1995). As our primary cultures do not contain dopaminergic cells of the substantia nigra pars compacta but should nevertheless permit normal MSN and circuit development, our cocultures provide us the unique opportunity to study how D_2R activation alters synaptic function. The use of transgenic mice that allow for live identification of two populations of neurons provides us an additional, straightforward internal control.

D_2R activation increases collateral frequency and strength

The rate of functional synaptic connectivity in our coculture model was consistently higher in D_2–D_2 MSN pairs than any other configuration. Despite the difference in frequency of functional synapses in basal conditions, eIPSC size and kinetics remained consistent between MSN pairs. Chronic D_2R activation with 72 h of 10 μM quinpirole treatment, however, increased both the rate and size of eIPSCs specifically in D_1–D_2 and D_2–D_2 pairs, suggestive of a postsynaptic mechanism of D_2R activation. This increase was not seen in pairs that had been treated with a combination of quinpirole and $D_{2/3}$ antagonist sulpiride, demonstrating that 10 μM quinpirole is effectively targeting D_2 MSNs.

Sholl analyses revealed that chronic D_2R activation increased both the number of primary dendrites and the dendritic arborization of D_2 MSNs. While this correlates with the increased number of functional synapses onto treated D_2 MSNs, it has recently been reported that chronic D_2R upregulation *in vivo* in the mouse increases MSN excitability and decreases dendritic arborization by the downregulation of inward rectifying potassium channels (Cazorla et al., 2012). There are several reasons underlying the divergence of our study from these results. It is likely that there are distinct intracellular pathways and compensatory mechanisms activated by D_2R upregulation compared with chronic D_2R activation. In addition, there are inherent differences in the *in vivo* versus *in vitro* the experimental settings. In fact, the number of primary dendrites of MSNs in dissociated cultures (4–6) is consistent with what has been previously reported, and is lower than what has been observed in slices (6–8;

Gertler et al., 2008). Day et al. (2006) provide evidence that DA depletion reduces primary dendrite number selectively in D_2 MSNs from six to four. In combination with the reported reduction in primary dendrites of corticostriatal cultures, which inherently lack DA input (Gertler et al., 2008), these two studies further support the idea that DA activation of D_2Rs regulates D_2 MSN morphology.

Coordinated presynaptic and postsynaptic mechanisms

Consistent with an increase in functional synapses onto D_2 MSNs, we observed an increase in presynaptic GABA sites and postsynaptic gephyrin clusters along D_2 MSN dendrites with quinpirole treatment. These results parallel the enhanced sensitivity to low concentrations of GABA in treated D_2 MSNs. However, the possibility of differential $GABA_A$ receptor subtype expression should also be considered.

The pharmacological dissection of native $GABA_A$ receptor subtypes is challenging because of the specificity of available modulators and heterogeneity of endogenous subunit expression. Based on reported expression studies by Pirker et al. (2000), striatal $GABA_A$ receptors should be predominantly composed of $\alpha2$, $\beta1/3$, and $\gamma2$ subunits. $\alpha1$, $\alpha4$, $\alpha5$, And δ subunits have been also shown to be expressed. Previous studies in our group have suggested that the presence of specific DA receptors in MSNs affect synaptic and extrasynaptic $GABA_A$ receptor function (Ade et al., 2008, Janssen et al., 2009), with a key role for $\beta3$ subunits (Janssen et al., 2011). The present results, however, show that the sensitivity to etomidate, a $\beta2/3$ subunit-containing agonist, does not change with chronic D_2R activation. Furthermore, currents in response to THIP, a superagonist of the extrasynaptic δ subunit-containing receptor (Brown et al., 2002), are unaltered by the treatment, suggesting the increase in GABA sensitivity is specific for synaptic receptors.

Our data show that diazepam prolongs the synaptic decay of GABA IPSCs in both nontreated and treated MSNs, but the actions on τ_w were enhanced in quinpirole-treated D_2 MSNs. This effect was observed to a greater degree on eIPSCs and not on mIPSCs; therefore, we conclude that this is a result of increased asynchronous summation of synaptic release from multiple sites. The possibility that mIPSCs and eIPSCs represented distinct inputs should be kept in mind when interpreting these results. It remains to be determined whether the increase in synaptic sites in treated D_2 MSNs is due to a morphological change in dendritic branching (Day et al., 2006), or whether it is due to a facilitation of $GABA_A$ receptor insertion at newly formed inhibitory synapses. The changes in dendritic morphology (Fig. 4) and the increased sensitivity of treated D_2 MSNs to low doses of GABA that parallels increases in gephyrin clusters (Fig. 7) support the hypothesis of a coordinated dopaminergic control of $GABA_A$ receptor clusters and dendritic morphology in D_2 MSNs. The effect of quinpirole treatment is selective for postsynaptic D_2 MSNs and independent from the presynaptic cell being D_1 or D_2 MSN. This supports the hypothesis that D_2R activation in postsynaptic D_2 MSNs has its effect through one of the multiple intracellular cascades that regulates $GABA_A$ receptor trafficking (Vithlani et al., 2011) and dendritic morphology (Day et al., 2008).

The role of D_2R is central in neuropsychiatric disorders. Our results begin to elucidate the powerful action of biochemical cascades following activation of these receptors in contributing to synapse formation and functionality (Girault and Greengard, 2004). We provide a model for future studies that may define the relative role of distinct components of this cascade, and compare the role of D_1 receptor activation. One must consider when comparing results of DA receptor stimulation that, while DA is released in a context-dependent manner *in vivo*, selective agonists are always present in culture. Prolonged agonist application may alter receptor signaling paradigms, potentially producing different effects compared with discontinuous stimulation.

Previous studies have shown that DA regulates the efficacy of MSN collaterals (Taverna et al., 2008). Our results extend these findings and provide an experimental assay to mechanistically analyze this effect. Together, our data suggest that DA D_2 receptor activation facilitates inhibitory synapse formation via coordinated presynaptic and postsynaptic changes.

References

Abi-Dargham A, Rodenhiser J, Printz D, Zea-Ponce Y, Gil R, Kegeles LS, Weiss R, Cooper TB, Mann JJ, Van Heertum RL, Gorman JM, Laruelle M (2000) Increased baseline occupancy of D2 receptors by dopamine in schizophrenia. Proc Natl Acad Sci U S A 97:8104–8109. CrossRef Medline

Ade KK, Janssen MJ, Ortinski PI, Vicini S (2008) Differential tonic GABA conductances in striatal medium spiny neurons. J Neurosci 28:1185–1197. CrossRef Medline

Albin RL, Young AB, Penney JB (1989) The functional anatomy of basal ganglia disorders. Trends Neurosci 12:366–375. CrossRef Medline

Asensio S, Romero MJ, Romero FJ, Wong C, Alia-Klein N, Tomasi D, Wang GJ, Telang F, Volkow ND, Rita RZ (2010) Striatal dopamine D2 receptor availability predicts the thalamic and medial prefrontal responses to reward in cocaine abusers three years later. Synapse 64:397–402. CrossRef Medline

Bekkers JM (2005) Presynaptically silent GABA synapses in hippocampus. J Neurosci 25:4031–4039. CrossRef Medline

Bolam JP, Hanley JJ, Booth PA, Bevan MD (2000) Synaptic organisation of the basal ganglia. J Anat 196:527–542. CrossRef Medline

Brown N, Kerby J, Bonnert TP, Whiting PJ, Wafford KA (2002) Pharmacological characterization of a novel cell line expressing human alpha(4)beta(3)delta $GABA_A$ receptors. Br J Pharmacol 136:965–974. CrossRef Medline

Cazorla M, Shegda M, Ramesh B, Harrison NL, Kellendonk C (2012) Striatal D2 receptors regulate dendritic morphology of medium spiny neurons via Kir2 channels. J Neurosci 32:2398–2409. CrossRef Medline

Chan CS, Peterson JD, Gertler TS, Glajch KE, Quintana RE, Cui Q, Sebel LE, Plotkin JL, Shen W, Heiman M, Heintz N, Greengard P, Surmeier DJ (2012) Strain-specific regulation of striatal phenotype in Drd2-eGFP BAC transgenic mice. J Neurosci 32:9124–9132. CrossRef Medline

Chuhma N, Tanaka KF, Hen R, Rayport S (2011) Functional connectome of the striatal medium spiny neuron. J Neurosci 31:1183–1192. CrossRef Medline

Churchill PS, Sejnowski TJ (1992) The computational brain. Cambridge, MA: MIT.

Clements JD, Silver RA (2000) Unveiling synaptic plasticity: a new graphical and analytical approach. Trends Neurosci 23:105–113. CrossRef Medline

Czubayko U, Plenz D (2002) Fast synaptic transmission between striatal spiny projection neurons. Proc Natl Acad Sci U S A 99:15764–15769. CrossRef Medline

Day M, Wang Z, Ding J, An X, Ingham CA, Shering AF, Wokosin D, Ilijic E, Sun Z, Sampson AR, Mugnaini E, Deutch AY, Sesack SR, Arbuthnott GW, Surmeier DJ (2006) Selective elimination of glutamatergic synapses on striatopallidal neurons in Parkinson disease models. Nat Neurosci 9:251–259. CrossRef Medline

Day M, Wokosin D, Plotkin JL, Tian X, Surmeier DJ (2008) Differential excitability and modulation of striatal medium spiny neuron dendrites. J Neurosci 28:11603–11614. CrossRef Medline

Dehorter N, Michel FJ, Marissal T, Rotrou Y, Matrot B, Lopez C, Humphries MD, Hammond C (2011) Onset of pup locomotion coincides with loss of NR2C/D-mediated cortico-striatal EPSCs and dampening of striatal network immature activity. Front Cell Neurosci 5:24. CrossRef Medline

Deyts C, Galan-Rodriguez B, Martin E, Bouveyron N, Roze E, Charvin D, Caboche J, Bétuing S (2009) Dopamine D2 receptor stimulation potentiates PolyQ-Huntingtin-induced mouse striatal neuron dysfunctions via Rho/ROCK-II activation. PloS One 4:e8287. CrossRef Medline

Farrant M, Nusser Z (2005) Variations on an inhibitory theme: phasic and

tonic activation of GABA(A) receptors. Nat Rev Neurosci 6:215–229. CrossRef Medline

Gerfen CR, Young WS 3rd (1988) Distribution of striatonigral and striatopallidal peptidergic neurons in both patch and matrix compartments: an *in situ* hybridization histochemistry and fluorescent retrograde tracing study. Brain Res 460:161–167. CrossRef Medline

Gertler TS, Chan CS, Surmeier DJ (2008) Dichotomous anatomical properties of adult striatal medium spiny neurons. J Neurosci 28: 10814–10824. CrossRef Medline

Girault JA, Greengard P (2004) The neurobiology of dopamine signaling. Arch Neurol 61:641–644. CrossRef Medline

Gittis AH, Kreitzer AC (2012) Striatal microcircuitry and movement disorders. Trends Neurosci 35:557–564. CrossRef Medline

Goffin D, Ali AB, Rampersaud N, Harkavyi A, Fuchs C, Whitton PS, Nairn AC, Jovanovic JN (2010) Dopamine-dependent tuning of striatal inhibitory synaptogenesis. J Neurosci 30:2935–2950. CrossRef Medline

Gong S, Zheng C, Doughty ML, Losos K, Didkovsky N, Schambra UB, Nowak NJ, Joyner A, Leblanc G, Hatten ME, Heintz N (2003) A gene expression atlas of the central nervous system based on bacterial artificial chromosomes. Nature 425:917–925. CrossRef Medline

Graybiel AM, Aosaki T, Flaherty AW, Kimura M (1994) The basal ganglia and adaptive motor control. Science 265:1826–1831. CrossRef Medline

Gustafson N, Gireesh-Dharmaraj E, Czubayko U, Blackwell KT, Plenz D (2006) A comparative voltage and current-clamp analysis of feedback and feedforward synaptic transmission in the striatal microcircuit *in vitro*. J Neurophysiol 95:737–752. Medline

Janssen MJ, Ade KK, Fu Z, Vicini S (2009) Dopamine modulation of GABA tonic conductance in striatal output neurons. J Neurosci 29:5116–5126. CrossRef Medline

Janssen MJ, Yasuda RP, Vicini S (2011) GABA(A) receptor β3 subunit expression regulates tonic current in developing striatopallidal medium spiny neurons. Front Cell Neurosci 5:15. CrossRef Medline

Johnson PM, Kenny PJ (2010) Dopamine D2 receptors in addiction-like reward dysfunction and compulsive eating in obese rats. Nat Neurosci 13:635–641. CrossRef Medline

Kapur S, Zipursky R, Jones C, Shammi CS, Remington G, Seeman P (2000) A positron emission tomography study of quetiapine in schizophrenia. Arch Gen Psychiatry 57:553–559. CrossRef Medline

Kaufman AM, Milnerwood AJ, Sepers MD, Coquinco A, She K, Wang L, Lee H, Craig AM, Cynader M, Raymond LA (2012) Opposing roles of synaptic and extrasynaptic NMDA receptor signaling in cocultured striatal and cortical neurons. J Neurosci 32:3992–4003. CrossRef Medline

Koos T, Tepper JM, Wilson CJ (2004) Comparison of IPSCs evoked by spiny and fast-spiking neurons in the neostriatum. J Neurosci 24: 7916–7922. CrossRef Medline

Kramer PF, Christensen CH, Hazelwood LA, Dobi A, Bock R, Sibley DR, Mateo Y, Alvarez VA (2011) Dopamine D2 receptor overexpression alters behavior and physiology in Drd2-EGFP mice. J Neurosci 31:126–132. CrossRef Medline

Kreitzer AC, Malenka RC (2008) Striatal plasticity and basal ganglia circuit function. Neuron 60:543–554. CrossRef Medline

Lieberman AN, Goldstein M (1985) Bromocriptine in Parkinson disease. Pharmacol Rev 37:217–227. Medline

Macdonald RL, Olsen RW (1994) GABAA receptor trafficking, channel activity, and functional plasticity of inhibitory synapses. Annu Rev Neurosci 17:569–602. Medline

Madisen L, Zwingman TA, Sunkin SM, Oh SW, Zariwala HA, Gu H, Ng LL, Palmiter RD, Hawrylycz MJ, Jones AR, Lein ES, Zeng H (2010) A robust and high-throughput Cre reporting and characterization system for the whole mouse brain. Nat Neurosci 13:133–140. CrossRef Medline

Mody I, De Koninck Y, Otis TS, Soltesz I (1994) Bridging the cleft at GABA synapses in the brain. Trends Neurosci 17:517–525. CrossRef Medline

Murase K, Ryu PD, Randic M (1989) Excitatory and inhibitory amino acids and peptide-induced responses in acutely isolated rat spinal dorsal horn neurons. Neurosci Lett 103:56–63. CrossRef Medline

Nusser Z, Naylor D, Mody I (2001) Synapse-specific contribution of the variation of transmitter concentration to the decay of inhibitory postsynaptic currents. Biophys J 80:1251–1261. CrossRef Medline

Partridge JG, Janssen MJ, Chou DY, Abe K, Zukowska Z, Vicini S (2009) Excitatory and inhibitory synapses in neuropeptide Y-expressing striatal interneurons. J Neurophysiol 102:3038–3045. CrossRef Medline

Pirker S, Schwarzer C, Wieselthaler A, Sieghart W, Sperk G (2000) GABA(A) receptors: immunocytochemical distribution of 13 subunits in the adult rat brain. Neuroscience 101:815–850. CrossRef Medline

Plenz D (2003) When inhibition goes incognito: feedback interaction between spiny projection neurons in striatal function. Trends Neurosci 26: 436–443. CrossRef Medline

Plenz D, Aertsen A (1996) Neural dynamics in cortex-striatum co-cultures—I. Anatomy and electrophysiology of neuronal cell types. Neuroscience 70:861–891. CrossRef Medline

Plenz D, Kitai ST (1998) Up and down states in striatal medium spiny neurons simultaneously recorded with spontaneous activity in fast-spiking interneurons studied in cortex-striatum-substantia nigra organotypic cultures. J Neurosci 18:266–283. Medline

Ramerstorfer J, Furtmüller R, Vogel E, Huck S, Sieghart W (2010) The point mutation gamma 2F77I changes the potency and efficacy of benzodiazepine site ligands in different GABAA receptor subtypes. Eur J Pharmacol 636:18–27. CrossRef Medline

Randall FE, Garcia-Munoz M, Vickers C, Schock SC, Staines WA, Arbuthnott GW (2011) The corticostriatal system in dissociated cell culture. Front Syst Neurosci 5:52. CrossRef Medline

Sassoè-Pognetto M, Panzanelli P, Sieghart W, Fritschy JM (2000) Colocalization of multiple $GABA_A$ receptor subtypes with gephyrin at postsynaptic sites. J Comp Neurol 420:481–498. CrossRef Medline

Seeman P, Chau-Wong M, Tedesco J, Wong K (1975) Brain receptors for antipsychotic drugs and dopamine: direct binding assays. Proc Natl Acad Sci U S A 72:4376–4380. CrossRef Medline

Segal M, Greenberger V, Korkotian E (2003) Formation of dendritic spines in cultured striatal neurons depends on excitatory afferent activity. Eur J Neurosci 17:2573–2585. CrossRef Medline

Shuen JA, Chen M, Gloss B, Calakos N (2008) *Drd1a*-tdTomato BAC transgenic mice for simultaneous visualization of medium spiny neurons in the direct and indirect pathways of the basal ganglia. J Neurosci 28:2681–2685. CrossRef Medline

Taverna S, Ilijic E, Surmeier DJ (2008) Recurrent collateral connections of striatal medium spiny neurons are disrupted in models of Parkinson's disease. J Neurosci 28:5504–5512. CrossRef Medline

Tecuapetla F, Carrillo-Reid L, Bargas J, Galarraga E (2007) Dopaminergic modulation of short-term synaptic plasticity at striatal inhibitory synapses. Proc Natl Acad Sci U S A 104:10258–10263. CrossRef Medline

Tian X, Kai L, Hockberger PE, Wokosin DL, Surmeier DJ (2010) MEF-2 regulates activity-dependent spine loss in striatopallidal medium spiny neurons. Mol Cell Neurosci 44:94–108. CrossRef Medline

Tunstall MJ, Oorschot DE, Kean A, Wickens JR (2002) Inhibitory interactions between spiny projection neurons in the rat striatum. J Neurophysiol 88:1263–1269. Medline

Vithlani M, Terunuma M, Moss SJ (2011) The dynamic modulation of GABA(A) receptor trafficking and its role in regulating the plasticity of inhibitory synapses. Physiol Rev 91:1009–1022. CrossRef Medline

Volkow ND, Chang L, Wang GJ, Fowler JS, Ding YS, Sedler M, Logan J, Franceschi D, Gatley J, Hitzemann R, Gifford A, Wong C, Pappas N (2001) Low level of brain dopamine D2 receptors in methamphetamine abusers: association with metabolism in the orbitofrontal cortex. Am J Psychiatry 158:2015–2021. Medline

Wilson CJ (1994) Understanding the neostriatal microcircuitry: high-voltage electron microscopy. Microsc Res Tech 29:368–380. CrossRef Medline

Zhou QY, Palmiter RD (1995) Dopamine-deficient mice are severely hypoactive, adipsic, and aphagic. Cell 83:1197–1209. CrossRef Medline

Zold CL, Kasanetz F, Pomata PE, Belluscio MA, Escande MV, Galinanes GL, Riquelme LA, Murer MG (2012) Striatal gating through up states and oscillations in the basal ganglia: implications for Parkinson's disease. J Physiol Paris 106:40–46. CrossRef Medline